Prospective Evaluation of Gaseous and Mineralized Dual CO$_2$ Sequestration in Mined-Out Area—A Case Study in Yu-Shen Coal Area

Jiangtao Zhai [1], **Liqiang Ma** [1,2,3,4,*], **Yujun Xu** [5], **Yangyang Wang** [6], **Kunpeng Yu** [1], **Zhiyang Zhao** [1], **Chengkun Peng** [1] and **Zhishang Zhang** [1]

[1] School of Mines, China University of Mining and Technology, Xuzhou 221116, China; tb21020005b3ld@cumt.edu.cn (J.Z.); tbh275@cumt.edu.cn (K.Y.); tb24020045a41ld@cumt.edu.cn (Z.Z.); ts23020041a31ld@cumt.edu.cn (C.P.); ts23020076a31@cumt.edu.cn (Z.Z.)

[2] Xinjiang Key Laboratory of Coal-Bearing Resources Exploration and Exploitation, Xinjiang Institute of Engineering, Urumqi 830023, China

[3] Xinjiang Engineering Research Center of Green Intelligent Coal Mining, Xinjiang Institute of Engineering, Urumqi 830023, China

[4] Key Laboratory of Xinjiang Coal Resources Green Mining (Xinjiang Institute of Engineering), Ministry of Education, Urumqi 830023, China

[5] State Key Laboratory of Digital Intelligent Technology for Unmanned Coal Mining, Anhui University of Science and Technology, Huainan 232001, China; xyj@aust.edu.cn

[6] DIMINE Co., Ltd., Changsha 410205, China; wyyang009@163.com

* Correspondence: ckma@cumt.edu.cn

Abstract

This research introduces a novel dual CO$_2$ storage (DCS) approach by simultaneously storing CO$_2$ gas in abandoned mines and securing it within mineralized backfill. For this method, CO$_2$ mineralized backfill materials (CMBM) are pumped into CO$_2$ mineralized storage segments (CMSSs) to support the roof while gaseous CO$_2$ is injected into gaseous CO$_2$ storage segments (GCSSs) to maximize storage amounts. This study focuses on the Yu-Shen coal area in Yulin City, Shaanxi Province, China. A three-level evaluation model was constructed to predict DCS feasibility based on the analytic hierarchy process (AHP) and fuzzy comprehensive assessment method. The model was generalized and applied to the whole coal area. Each indicator affecting adaptability is plotted on a thematic map to determine the corresponding membership degree. The aptness for 400 boreholes distributed in the entire area was derived and a zoning map which divides the whole area into different suitability was drawn. This paper puts forward a mathematical model for predicting DCS suitability. The findings establish an engineering paradigm that simultaneously addresses CO$_2$ sequestration, industrial waste recycling, and ecological water table preservation. The research results can provide references for determining the site of DCS, contributing to the generalization of DCS in a larger range.

Keywords: dual CO$_2$ storage (DCS); feasibility; AHP–fuzzy comprehensive evaluation; CO$_2$ mineralized backfill materials

1. Introduction

The Global Carbon Project from an international non-government organization shows that worldwide CO$_2$ emissions totaled 37.8 billion tons in 2024. Rapid industrialization has substantially increased China's contribution, now accounting for approximately one-quarter of the global total [1]. Such extensive emissions drive critical issues like sea-level

rise, freshwater depletion, and extreme weather patterns [2], creating significant risks for ecosystems, public health, and human livelihoods. Consequently, developing efficient carbon mitigation solutions is critically urgent [3,4].

The long-term geological sequestration of carbon dioxide, including in depleted reservoirs, goafs, and other deep geological formations, as well as the deep ocean, presents a viable strategy for climate change mitigation; this approach lowers atmospheric greenhouse gas concentrations to advance environmental protection and safeguard ecosystem health [5–7]. Coal-fired power plants are major CO_2 emitters, often situated near numerous abandoned coal mines [8]. China alone anticipates approximately 15,000 such mines by 2030. While technical and economic constraints have hindered the utilization of these mines' residual coal resources and deep underground voids, these sites offer significant potential for CO_2 storage [9]. Significant global research focuses on forecasting CO_2 sequestration suitability. Machine learning techniques are prominent, with studies applying algorithms to predict saline aquifer storage performance [10,11] and utilizing neural networks coupled with support vector machines to estimate essential CO_2 properties [12]. Numerical simulation methods have been employed to assess storage capacity in specific geological settings, such as a Vietnamese fractured basement reservoir [13]. Further site evaluations investigate storage potential near existing oil fields [14], appraise Indonesian coal seams for combined CO_2 storage and methane recovery enhancement [15], and apply predictive models to CO_2-enhanced oil recovery outcomes in residual oil zones [16]. Additionally, comparative analyses of fuzzy decision-making techniques for geological storage site selection have been conducted in specific regions [17].

Another feasible solution is CO_2 mineral carbonation backfill [18–20], which adsorbs CO_2 onto coal-derived solid wastes for permanent CO_2 storage alongside water-preserving coal mining [21,22]. Current studies are restricted in laboratory settings and concentrate on high temperature, high pressure, high-calcium fly ash (FA), and steam addition conditions to improve the CO_2 absorbing rate [23–26]. The raw materials include cement-based materials, FA, coal gangue (CG), and modified magnesium–coal-based solid waste [27–30]. However, the relatively slow CO_2 uptake rate of CMBM under ambient conditions for large-scale applications limits the efficiency of this approach [31,32]. To address this limitation, an enhanced method of DCS was developed, drawing inspiration from strip mining together with CO_2 carbonation backfill and CO_2 sequestration in abandoned mines [33]. This method involves dividing the whole DCS area into alternating sections designated for GCSS and CMSS. It can address green mining goals by simultaneously tackling excess CO_2, enabling safe disposal of coal waste, and protecting overlying aquifers and surface structures. By optimizing the width of CGSS (WGCSS) and CMSS (WCMSS), the goal of maximizing the benefits of CO_2 storage and minimizing ecological damage and ensuring safety can be achieved [34].

However, the practical implementation of this concept faces challenges due to complex mine engineering and hydrogeological conditions, alongside specific CMBM characteristics [35,36]. Multiple factors constrain DCS, including DCS site, hydrogeological conditions, geological structures, and DCS process systems. Consequently, systematically evaluating these diverse influencing factors through a comprehensive method is essential for predicting DCS feasibility across different mines. Common evaluation techniques include the AHP, Delphi method, weighted mean, fuzzy comprehensive evaluation, principal component analysis, and BP neural networks [37]. AHP, developed by Professor Saaty, is a widely adopted qualitative–quantitative decision-making tool for multi-objective or multi-scheme analysis across various sectors [38,39]. Herein, an AHP–fuzzy comprehensive evaluation model will be constructed to predict the adaptability of the DCS concept [40]. This model will be generalized and applied within the Yu-Shen mining area. Thematic maps illustrating

the spatial distribution of each influencing factor's membership degree across the coal area will be generated. Combining these membership degrees with factor weights will yield a comprehensive evaluation value Φ indicating the adaptability grade for 400 boreholes in the Yu-Shen area. The entire region will then be classified into four suitability categories: good, moderate, slightly poor, and poor.

This paper introduces the concept of DCS, which uses CMSS to support overlying rocks and GCSS to maximize CO_2 storage amounts. The prediction model for DCS suitability offers a theoretical foundation for future implementation in coal mines, supporting the transition towards green and sustainable mining practices.

2. Operating Process of DCS

The DCS utilizing three mining roadways (MRs) is illustrated through conceptual and procedural diagrams (Figures 1 and 2).
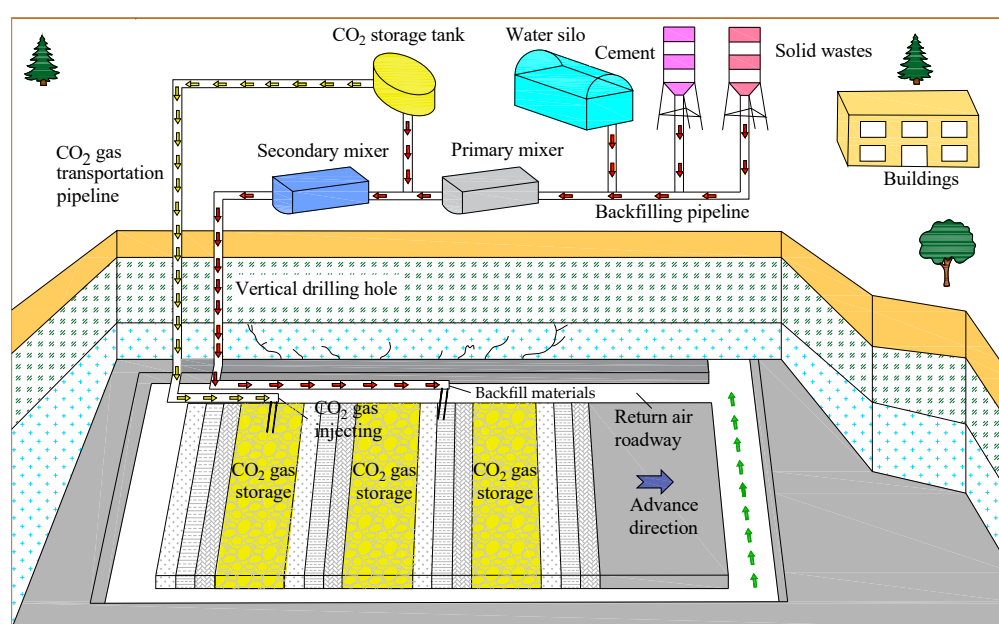

Figure 1. Three-dimensional overview of DCS.

Initially, the DCS zone is partitioned into alternating CMSSs (S_1, S_2, S_3, ..., S_m) and GCSSs (G_1, G_2, G_3, ..., G_m) along the strike direction. Each CMSS is subdivided into i MRs ($3 \leq i \leq 5$). Coal extraction from MRs is performed using continuous miners, while concurrently producing CMBM by blending CO_2 with coal-derived solid wastes like FA and CG. This CMBM is promptly pumped into the excavated MR goaf, with simultaneous extraction of the subsequent ($i-1$) MRs in the same phase. Once all MRs within the initial phase are mined and filled, subsequent phases repeat this process until the entire CMSS is replaced by CMBM. Next, the Wongawilli rapid mining technique is applied to extract coal from the GCSS. Following roof collapse and stabilization post-extraction, high-pressure CO_2 is injected into the GCSS goaf. This gas backfilling process is replicated sequentially across all GCSSs until the entire area is filled with pressurized CO_2. Throughout this workflow, concurrent operations ensure continuous extraction and backfilling cycles across alternating CMSSs and GCSSs.

The injection is implemented in staged campaigns, beginning with a pilot to assess near-field response and then progressively scaling up. Injection pressure and flow are kept below the local fracture gradient and tailored to the permeability and stress conditions of the target goaf to prevent unintended fracturing. Continuous monitoring should combine wellhead and downhole pressure and temperature sensors, flowmeters, and periodic gas

composition analyses with subsurface surveillance using microseismic arrays, borehole logging, and geophysical surveys; surface displacement is tracked by InSAR and GPS, while groundwater and soil gas sampling evaluate environmental impacts. Coupled reservoir geomechanics modeling, supported by sensitivity analyses, will guide the selection of injection rates and monitoring locations. Predefined contingency measures (e.g., shut-in, depressurization, remediation) and trigger thresholds are established to protect operational safety and long-term stability.
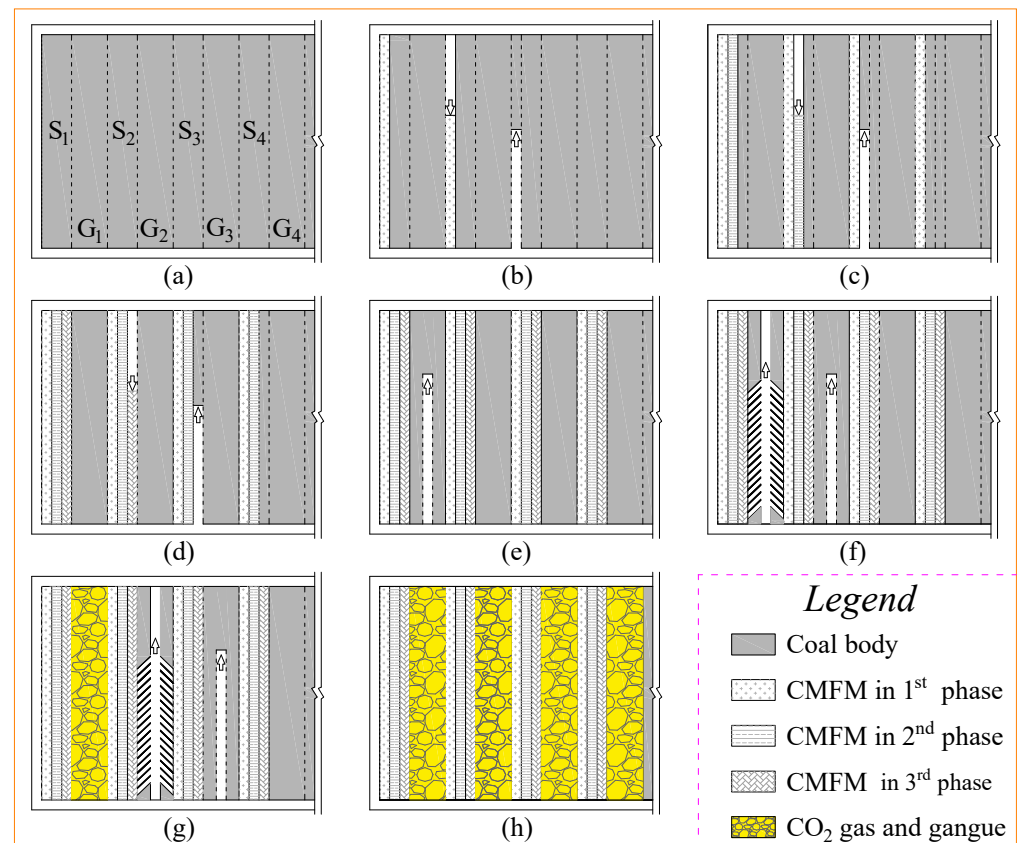

Figure 2. Operating processes of DCS. (**a**) Layout of the CMSS and GCSS; (**b**) The MR in 1st phase of CMSS is being excavated; (**c**) The MR in 2nd phase of CMSS is being excavated; (**d**) The MR in 3rd phase of CMSS is being excavated; (**e**) The MR of GCSS is being excavated; (**f**) The GCSS is being extracted using the Wongawilli rapid mining technique.; (**g**) The GCSS is being injected with CO_2; (**h**) All GCSS is injected with CO_2.

3. Determination of Indicators and Membership Functions

The factors governing the suitability of DCS are numerous and imprecise, fitting naturally with the concepts of fuzzy mathematics. By combining the analytic hierarchy process (AHP) with fuzzy comprehensive evaluation, these nebulous factors can be translated into quantitative measures, improving clarity and reliability.

Using this combined approach, a three-tiered framework was established and relative weights for each indicator were derived. This model groups indicators into four secondary categories: DCS site characteristics, hydrogeological conditions, geological–structural features, and DCS operational/process parameters. A set of twelve tertiary indicators was defined—for example, site burial depth, allowable storage height, strength of floor strata, nature of overlying beds, distance from the aquifer to the site, and the vertical position of any aquifuge, as shown in Figure 3. Membership functions for all indicators were calibrated based on on-site experience and a comprehensive literature survey to ensure practical relevance and theoretical support.
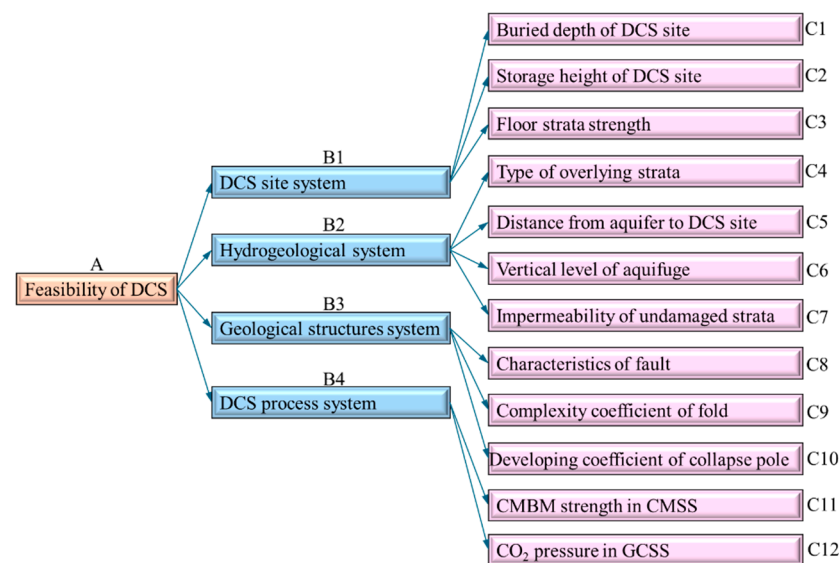
Figure 3. Indicators affecting DCS suitability.

3.1. DCS Site System

3.1.1. Depth of DCS Site (b)

Determining optimal depths for CO_2 sequestration in abandoned mine voids necessitates rigorous evaluation of leakage pathways, phase behavior, and geological confinement. Within shallow subsurface zones (<200 m), CO_2 persists primarily in low-density gaseous or subcritical liquid states, elevating escape risks. This configuration mandates engineered containment barriers to depress porosity and is coupled with precise pressure regulation. The intermediate depth band (800–1500 m) demonstrates superior viability: CO_2 transitions to a supercritical phase (600–900 kg/m^3 density), substantially diminishing buoyancy-driven migration. Inherent caprock integrity (fracture thresholds >12 MPa) provides additional migration resistance [41]. Deeper goafs (>1500 m) present heightened fault-mediated leakage hazards, necessitating integrated "buffer-isolation" strategies. The 800–1500 m horizon is designated the prime target for commercial-scale storage, harmonizing phase stability, retention efficiency, and technical feasibility, whereas deeper implementations greater than 2400 m demand specialized materials or systemic adaptations to manage inherent vulnerabilities. Hence, the membership function of the DCS depth b is

$$\mu_{1a}(b) = \begin{cases} 0, & b \leq 200 \\ (b-200)/600, & 200 < b \leq 800 \\ 1, & 800 < b \leq 1500 \\ (2400-b)/900, & 1500 < b \leq 2400 \\ 0, & b > 2400 \end{cases} \tag{1}$$

3.1.2. Height of DCS Site (h)

For CO_2 goaf storage, coal seam thickness selection must balance fracture zone development and containment safety. Medium-thick seams (8–12 m) are prioritized, exhibiting fracture heights (H_f) of 18 times the mining height (144–216 m). This optimizes storage capacity while enabling effective containment via natural or engineered seals. Thin seams (<5 m), with limited fracture zones (<90 m), serve only as regional supplements considering storage potential. Conversely, thick seams (>15 m) offer substantial capacity but

develop elevated fracture zones (>300 m), necessitating height-limited extraction and robust engineered seals.

$$\mu_{1b}(h) = \begin{cases} 0, & h \leq 5 \\ (h-5)/3, & 5 < h \leq 8 \\ 1.0, & 8 < h \leq 12 \\ (15-h)/3, & 12 < h \leq 15 \\ 0, & h \geq 15 \end{cases} \tag{2}$$

3.1.3. Floor Strength of DCS Site (F_s)

The floor strength thresholds are dynamically governed by DCS depth and CO_2 injection pressures. Field data from Shanxi mines indicate that at shallow depths ranging from 100 to 300 m, floor strata require UCS greater than 20 MPa to withstand typical CO_2 injection pressures (4–10 MPa) without plastic deformation. For mid-depth goafs from 300 to 1000 m, elevated geostatic stresses necessitate UCS surpassing 30 MPa to limit deformation to less than 0.1‰. Numerical models confirm that floors with UCS less than 20 MPa risk tensile fracturing under CO_2 pressures exceeding 6 MPa, particularly when traversed by through-going discontinuities. Reinforcement strategies for substandard floors—such as silicate grouting boosting UCS by 30–50% or concrete barriers—demonstrate efficacy, evidenced by Huangling's successful sequestration of 3.569×10^6 kg CO_2 in high-strength floors (UCS > 30 MPa) and Changcun's minimal deformation in sandy mudstone with UCS varying from 35 to 60 MPa under operational pressures.

$$\mu_{1c}(F_s) = \begin{cases} 0, & F_s \leq 20 \\ (F_s-20)/25, & 20 < F_s \leq 45 \\ 1, & F_s > 45 \end{cases} \tag{3}$$

3.2. Hydrogeological System

3.2.1. Overburden Type (O_t)

The lithological composition of overburden fundamentally governs the evolution of water-conducting fractures. Brittle, hard rock formations exhibit sudden structural failure, promoting widespread fracture propagation. In contrast, soft lithologies experience progressive compaction during extraction, diminishing fracture heights via mechanical closure mechanisms. Hydro-weakening amplifies plastic deformation and clay-mineral transformation (argillization) in these strata, enhancing fracture sealing and permeability resistance. Mobilized argillaceous particulates further obstruct fracture pathways in subjacent units. Hydro-expansive soft formations demonstrate volumetric swelling upon hydration, mechanically reclosing discontinuities and fragmenting fracture network connectivity. Stratigraphic alternation of rigid and ductile units capitalizes on complementary properties: hard layers constrain deformation, while soft strata block fluid migration, achieving optimal fracture containment efficacy.

$$\mu_{2a}(O_t) = \begin{cases} 0, & Broken\ strata \\ 0.6, & Hard\ strata \\ 0.8, & Soft\ strata \\ 1.0, & Composited\ strata \end{cases} \tag{4}$$

3.2.2. Distance from Aquifer to DCS (L_d)

Hydrogeological isolation efficacy depends critically on the interval between mining horizons and overlying aquifers. Where the interburden thickness exceeds the com-

bined height of the water-conducting fracture network and protective stratum thickness, aquicludes completely prevent hydraulic communication between the aquifer and DCS site. When this separation merely surpasses the fracture zone height, groundwater experiences restricted vertical migration through the intervening strata without inducing inrush hazards. Conversely, interburden dimensions below the fracture zone elevation permit direct hydraulic connectivity, enabling aquifer depletion and potentiometric surface decline. Under such conditions, the system fundamentally compromises both DCS and water resource preservation objectives.

To prevent aquifer infiltration and inrush, the protective zone thickness between the fracture zone ceiling and the aquifer must be quantified using stratum-specific water-resisting indices. Clay strata greater than 12 m can block aquifer seepage. Considering the safety coefficient, the protection zone thickness is 18 m.

$$\mu_{2b}(L_d) = \begin{cases} 0, & L_d \leq H_f \\ \left(L_d - H_f\right)/18, & H_f < L_d \leq H_f + 18 \\ 1, & L_d > H_f + 18 \end{cases} \tag{5}$$

where d denotes the distance from the overlying aquifer to the DCS site, m; H_f denotes the height of the water-conducting fractured zone (HWCFZ), m; and T_p denotes the thickness of the protective zone.

3.2.3. Vertical Level of Low-Permeability Caprock (V_c)

Low-permeability caprock (aquifuge) is fundamental to ensuring the security of DCS, with its efficacy relying on the vertical position of the aquifuge. The immediate primary caprock, adjacent to the DCS site, serves as the foremost barrier, directly impeding CO_2 vertical migration and determining storage capacity by virtue of its high capillary entry pressure and mechanical integrity. The overlying intermediate seal units act as a secondary defense; their multi-layered, heterogeneous structure increases the tortuosity of the CO_2 migration path, effectively retarding its ascent and promoting dissolution and mineral trapping. The uppermost regional seal constitutes the ultimate barrier protecting shallow freshwater resources and the biosphere.

$$\mu_{2c}(V_c) = \begin{cases} 0, & V_c = Low \\ 0.5, & V_c = Medium \\ 1, & V_c = High \end{cases} \tag{6}$$

3.2.4. Equivalent Permeability of Undamaged Strata (K_e)

The equivalent permeability coefficient of intact strata after DCS operations critically determines groundwater and CO_2 containment efficacy, with lower values indicating reduced escaping risk of water and gas. Previous studies established that 18 m clay strata effectively prevents aquifer infiltration, while 40 m clay achieves complete seepage isolation. Comparatively, mudstone-to-sandstone lithologies exhibit progressively diminished water-blocking capacity. The equivalent permeability coefficient is

$$K_e = \frac{H}{H_1/K_1 + H_2/K_2 + \ldots + H_n/K_n} = H / \left(\sum_{i=1}^{n} (H_i/K_i) \right) \tag{7}$$

where K_e and H denote the equivalent permeability coefficient and the thickness of the undamaged strata; H_i and K_i are the thickness and permeability coefficient of the *i-th* overlying layer in undamaged strata.

The seepage transit time through the undamaged strata H/K_e was selected as the indicator:

$$\mu_{2c}(K_e) = \begin{cases} 0, & H/K_e \leq 9 \times 10^8 \\ (H/K_e - 9 \times 10^8)/1.1 \times 10^9, & 9 \times 10^8 < H/K_e \leq 2 \times 10^9 \\ 1, & H/K_e > 2 \times 10^9 \end{cases} \tag{8}$$

3.3. Geological Structures System

3.3.1. Fault Strength (S)

Faults compromise overburden structural coherence, inducing distinct operational constraints. Medium–small discontinuities fragment strata near failure planes, risking overburden integrity during DCS. Major faults necessitate site layout modifications and trigger permanent protective coal pillars, reducing CO_2 storage potential. Hence, fault strength is quantified as the critical evaluation metric:

$$S = \sum_{i=1}^{n} L_i F_i / A \tag{9}$$

where L_i refers to the length of the *i-th* fault (m); F_i refers to the fault throw of the *i-th* fault (m); and A and n refers to the acreage and faults number over the DCS site, respectively.

The membership function of fault strength is

$$\mu_{3a}(S) = \begin{cases} 1, & S < 0.15 \\ (5 - 20S)/2, & 0.15 \leq S \leq 0.25 \\ 0, & S > 0.25 \end{cases} \tag{10}$$

3.3.2. Complexity Coefficient of Fold (p)

Tectonically folded strata exhibit high residual stress and accumulated strain energy. During CO_2 injection operations in GCSSs, this stored energy releases abruptly, potentially triggering structural compromise and violent strain energy release events in surrounding rock. Fold development complexity further affects the layouts and sequence of DCS, necessitating the fold complexity coefficient p as the critical evaluation metric.

$$p = \frac{w \cdot \Delta h}{l \cdot s} \tag{11}$$

where Δh is the elevation differential of DCS, m; w is the contour azimuthal variation, rad; l is the horizontal span of DCS, m; and s is the panel areal extent, km^2.

$$\mu_{3b}(p) = \begin{cases} 1, & p \leq 0.33 \\ \exp^{-(\frac{p-0.33}{0.33})^2}, & p > 0.33 \end{cases} \tag{12}$$

3.3.3. Development Coefficient of Collapsed Pole (K_v)

The development coefficient K_v of collapse columns serves as a critical indicator of infill compactness. Its determination requires comprehensive considerations of containment integrity and long-term stability. Experimental studies demonstrate that $K_v \geq 0.8$ represents the threshold for secure CO_2 storage without leakage, wherein the porosity of fragmented rock masses typically remains below 10%, and permeability coefficients can be controlled at an ultralow level ($<10^{-7}$ m/s). Conversely, $K_v < 0.8$ indicates substantial voids or loosely compacted infill (porosity > 25%), resulting in sharply elevated permeability and uncontrollable leakage risks. Such columns should be excluded from potential storage

reservoirs. For the transitional range from 0.5 to 0.8, grouting reinforcement is necessary to enhance compaction, supplemented by rigorous validation of auxiliary parameters—including permeability ($<10^{-6}$ m/s), fracture intensity (Rock Quality Designation > 70%), and hydraulic conductivity (specific capacity <0.1 L/s·m)—to ensure caprock integrity.

$$\mu_{3c}(K_v) = \begin{cases} 0, & K_v < 0.5 \\ (10K_v - 5)/3, & 0.5 \le K_v \le 0.8 \\ 1, & K_v > 0.8 \end{cases} \tag{13}$$

3.4. DCS Process System

3.4.1. CMBM Strength in CMSS (P_f)

CMBM serves as a support to overlying strata. Its unconfined compressive strength (UCS) controls the overburden displacement and fracture propagation and is therefore significant for DCS. The UCS is modulated by compositional parameters, i.e., mixture ratios, water–solid proportion, curing time, etc. The 56-day cured specimens exhibiting stable strength establish this benchmark as the evaluation metric.

$$\mu_{4a}(P_f) = \begin{cases} 0, & P_f \le 2.0 \\ (P_f - 2)/2, & 2.0 < P_f \le 4.0 \\ 1, & P_f > 4.0 \end{cases} \tag{14}$$

3.4.2. CO_2 Pressure in GCSS (P_r)

For CO_2 gaseous sequestration in GCSSs, operational confinement pressures should be rigorously maintained at 0.5–5 MPa to preserve subcritical phase conditions ($P_r < 7.38$ MPa) and ensure geomechanical stability. This operational window harmonizes storage efficacy with hazard control: shallow reservoirs (<500 m) employ 0.5–2 MPa pressures to curtail advective–diffusive losses, whereas deeper systems (500–1000 m) implement 2–5 MPa to augment CO_2 density (50–300 kg/m^3) whilst remaining below 80% of caprock tensile strength thresholds (typically 6–9 MPa for argillaceous formations) and 70% of minor fault reactivation pressures (2–3.5 MPa).

$$\mu_{4b}(P_r) = \begin{cases} 1, & P_r < 0.5 \\ (5 - P_r)/4.5, & 0.5 \le P_r \le 5 \\ 0, & P_r > 5 \end{cases} \tag{15}$$

4. Mathematical Modeling and Weight Distribution

4.1. Mathematical Modeling

The DCS suitability was assessed using an integrated AHP and fuzzy comprehensive evaluation methodology. This approach first identified the key factors affecting applicability, resulting in the definition of four sub-factors and ten tertiary-level factors. Within the established AHP framework, level A corresponds to the primary objective, level B signifies the evaluation criteria, and level C represents the sub-criteria. A judgment matrix was developed based on this hierarchical structure to numerically quantify and express the suitability assessment. All identified factors were then incorporated into a universe of discourse, denoted as *U*.

$$U = \{u_1, u_2, u_3, u_4, u_5, u_6\} \tag{16}$$

The universe of discourse for applicability is denoted as *V*. The comprehensive evaluation value Φ serves as the indicator for the adaptability grade. This value represents the membership degree of the evaluation factors (within domain *U*) belonging to the fuzzy subset *V*. Equation (17) defines this fuzzy subset *V* as follows:

$$V = \{\text{I, II, III, IV}\} \tag{17}$$

Φ is calculated using the following expression:

$$\Phi = \sum_{i=1}^{n} w_i u_i(u_i) \tag{18}$$

where $u_i(u_i)$ signifies the membership degree associated with the *i*-th factor, and w_i represents the weight assigned to the *i*-th indicator.

As outlined in Table 1, the fuzzy subset *V* categorizes the adaptability of DCS into four distinct grades. Hence, the calculated Φ value quantitatively represents the level of applicability.

Table 1. Classification standard for predicting the adaptability of DCS.

Grade	Feasibility Level	Φ	Description
I	High	$0.9 < \Phi < 1.0$	Implementation is fully viable at the mine site, delivering significant ecological, social, and economic returns.
II	Moderate	$0.8 < \Phi \le 0.9$	DCS can proceed with minor adjustments, yielding substantial benefits.
III	Marginal	$0.7 < \Phi \le 0.8$	Limited suitability exists due to complex engineering or hydrogeological constraints. Implementation requires significant mitigation measures and yields reduced returns.
IV	Low	$0.6 < \Phi \le 0.7$	Application is fundamentally unfeasible regardless of corrective actions. Despite enabling minimal CO_2 storage, the filling capacity is inadequate. Costs substantially outweigh benefits, resulting in financial non-viability.

4.2. Weight Distribution

The weights assigned to factors within a comprehensive evaluation system quantitatively define their structural relationships. These weights signify the comparative significance of each influencing element in the overall evaluation framework and are essential for aligning the system's structure with its intended function. To establish these weights, a pairwise comparison approach is employed. This involves systematically comparing each factor against every other factor to build a discriminant matrix (Equation (19)). Within this matrix, an entry z_{ij} (using a scale of 1 to 9 or their reciprocals) indicates the relative priority of factor *i* over factor *j* concerning a specific criterion. A higher z_{ij} value denotes greater perceived importance of factor *i* relative to *j*. The validity of the resulting matrix is subsequently evaluated using the maximum eigenvalue technique. Drawing upon prior research insights and incorporating expert assessments through structured scoring, the author formulated the subsequent discriminant matrix (Table 2).

$$W = (z_{ij})_{n \times n} = \begin{bmatrix} 1 & z_{12} & \cdots & z_{1n} \\ 1/z_{12} & 1 & \cdots & z_{2n} \\ \cdots & \cdots & \cdots & \cdots \\ 1/z_{1n} & 1/z_{2n} & \cdots & 1 \end{bmatrix} \tag{19}$$

Table 2. Comparison discriminant matrix.

Hierarchy	A-B	B$_1$-C	B$_2$-C
Matrix	$W_{A\sim B} = \begin{bmatrix} 1 & 2 & 1/3 & 3 \\ 1/2 & 1 & 1/5 & 3/2 \\ 3 & 6 & 1 & 8 \\ 1/3 & 2/3 & 1/8 & 1 \end{bmatrix}$	$W_{B_1\sim C} = \begin{bmatrix} 1 & 4 & 1/2 \\ 1/4 & 1 & 1/8 \\ 2 & 8 & 1 \end{bmatrix}$	$W_{B_2\sim C} = \begin{bmatrix} 1 & 2 & 1/2 & 1/3 \\ 1/2 & 1 & 1/4 & 1/6 \\ 2 & 4 & 1 & 3/4 \\ 3 & 6 & 3/2 & 1 \end{bmatrix}$
Hierarchy	B$_3$-C	B$_4$-C	
Matrix	$W_{B_3\sim C} = \begin{bmatrix} 1 & 3 & 2 \\ 1/3 & 1 & 3/4 \\ 1/2 & 4/3 & 1 \end{bmatrix}$	$W_{B_4\sim C} = \begin{bmatrix} 1 & 1/2 \\ 2 & 1 \end{bmatrix}$	

Taking $W_{A\sim B}$ as an example to illustrate the calculation processes of the model.

The first step: The largest eigenvalue and corresponding eigenvector calculation. First, calculating the *n-th* power root of obtain using $V_i = \sqrt[n]{\prod\limits_{j=1}^{n} z_{ij}}(i,j = 1,2,\ldots n)$; second, normalize using $W_i = V_i/\sum V_i$; third, determine the eigenvector of the judgment matrix using $W_i = (W_1, W_2, \ldots, W_n)$; finally, calculate the maximum eigenvalue of the matrix using $\lambda_{\max} = \dfrac{1}{n}\sum\limits_{i=1}^{n}\dfrac{(RW)_i}{W_i}$.

The calculation yields a maximum eigenvalue of 4.0503. The corresponding eigenvector is W = (0.2092, 0.1095, 0.6095, 0.0718).

The second step: Following the calculation of the discriminant matrix, its consistency is assessed using the consistency ratio (*C.R.* = *C.I./R.I.*). The consistency index *C.I.* is derived from the formula $(\lambda_{\max} - n)/(n - 1)$, where $\lambda_{\max}$ represents the matrix's largest eigenvalue and *n* is its order. *R.I.* denotes Saaty's random consistency index.

A matrix is considered consistent if *C.R.* < 0.1; otherwise, adjustments are necessary. The computed *C.R.* values for the matrices are 0.017, 0, 0.001, 0.010, and 0 (noting that *C.R.* is inherently 0 for matrices of order *n* < 2). Since all values fall below the 0.10 threshold, the judgment matrices and their resultant weights demonstrate satisfactory consistency. Subsequently, the weights for each influencing factor were computed based on their respective discriminant matrices (W_i). The calculated weights for all factors and sub-factors are as follows:

$$W_{A\sim B}(B_1, B_2, B_3, B_4) = (0.2092, 0.1095, 0.6095, 0.0718)$$
$$W_{B_1\sim C}(C_1, C_2, C_3) = (0.3077, 0.0769, 0.6154)$$
$$W_{B_2\sim C}(C_4, C_5, C_6, C_7) = (0.1524, 0.0762, 0.3140, 0.4573)$$
$$W_{B_3\sim C}(C_8, C_9, C_{10}) = (0.5472, 0.1897, 0.2631)$$
$$W_{B_4\sim C}(C_{11}, C_{12}) = (0.3333, 0.6667)$$

5. Generalization and Application of Prediction Model

Located north of Yulin City, Shaanxi Province, China, the Yu-Shen coal area encompasses 5160 km^2 and holds in situ coal reserves exceeding 30 billion tons. Initial large-scale mining drastically depleted the Salawusu Formation aquifer and surface water, severely impacting local water supplies and ecosystems. Mining-induced subsidence also caused significant surface damage, forcing village relocations and making backfill mining essential. Concurrently, coal operations and local power generation cause substantial solid waste (FA, CG) and CO$_2$ emissions. Hence, Yu-Shen is being studied to assess the potential suitability of DCS for future feasibility, though it remains unimplemented there. Prior to deployment, the proposed evaluation model was used to assess DCS adaptability across 400 borehole sites. The thematic Φ contour maps for planning were generated under different parameters. The Φ calculation involves three steps: First, thematic maps are created for

each individual indicator. Second, the membership degree for each factor is determined by analyzing these maps alongside the relevant literature. Third, the factor weights and the derived membership degrees are used to calculate Φ.

5.1. Membership Degree Determination

5.1.1. DCS System

Within the coal-bearing Jurassic Yan'an Formation, five principal coal seams are minable. These seams dip gently at angles between 1° and 3°. The thickness of the primary seam (height of DCS area) exhibits significant variation, from absence (0 m) up to 14 m. Across the entire region, the burial depth of the DCS site shallows progressively from west to east, reaching a maximum depth of approximately 700 m in the west (Figure 4). The floor strata consist mainly of sandy mudstone, mudstone, and carbonaceous mudstone. Lens-shaped bodies of marl occur sporadically within this floor sequence. The UCS of the floor rocks varies from 24 to 66 MPa, averaging 45 MPa. The structural complexity of the entire Yu-Shen coal area is low, with only seven minor faults detected. There are no significant fold or collapse column structures in the coal area.
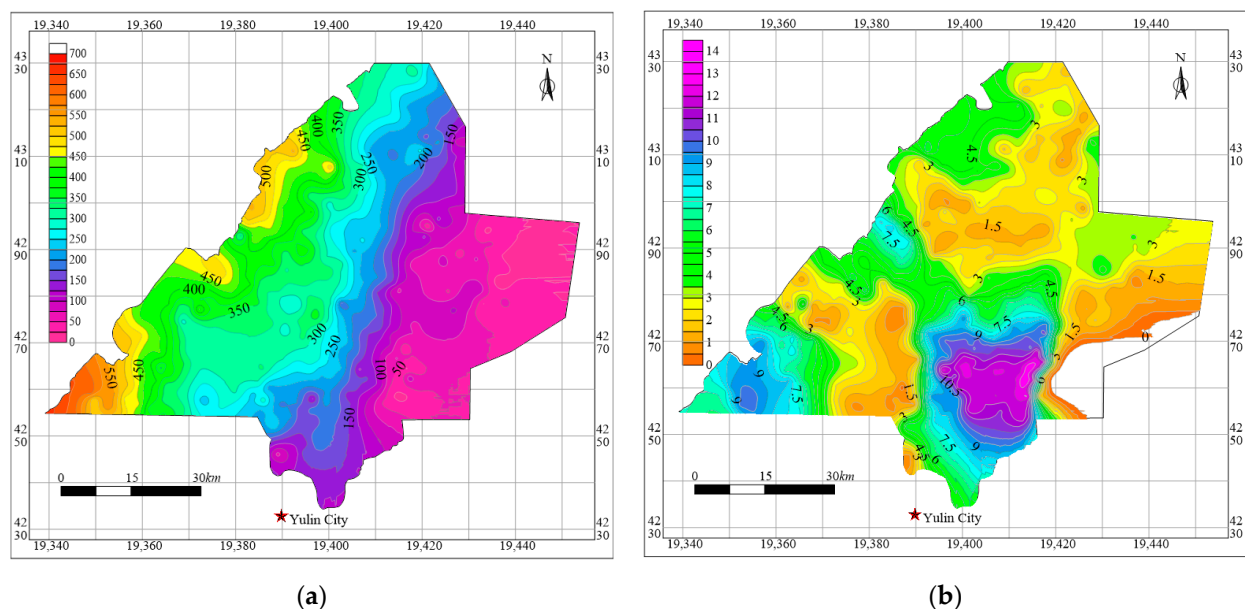

(**a**)　　　　(**b**)

Figure 4. Contour maps of DCS system. (**a**) Depth of DCS; (**b**) height of DCS.

5.1.2. Hydrogeological System

(1)　Overburden type

Based on spatial relationships and lithologic combinations within the overburden, the stratigraphic structure of the Yu-Shen coal area is classified into five types: (I) sand–soil–bedrock, (II) sand–bedrock, (III) bedrock, (IV) soil–bedrock, and (V) burnt rock [34]. Type I features sand, an aquitard (water-resisting soil layer), and bedrock. Type IV comprises an impermeable soil layer (primarily Lishi Formation loess and Baode Formation clay) overlying bedrock. Both Type I and IV exhibit upper soft layers above harder bedrock. Type III consists solely of bedrock exposed at the surface. Consideration for water percolation into DCS is unnecessary due to the very low yield of the porous bedrock-confined aquifer. Type II contains a sand phreatic aquifer directly over bedrock without an intervening continuous clay aquiclude. The substantial bedrock thickness above coal seams designates this structure as a key zone for DCS. Type I, II, and IV are characterized by composite strata while Type IV is solely hard rock. The burnt rock overburden resulting from coal seam self-ignition is thoroughly fractured and possesses high initial porosity. Mining-induced

fracture development and permeability degradation lead to direct hydraulic connectivity between the DCS site and aquifer.

(2)   Hydrogeological conditions

Four vertically sequenced aquifers (ascending order) occur in the study area, i.e., confined porous bedrock, burnt rock phreatic, Salawusu phreatic, and unconsolidated porous phreatic. Given the significant thickness (up to 67.3 m) and broad spatial extent (4000 km^2), the Salawusu Formation constitutes the principal aquifer requiring integration into DCS adaptability predictions. Utilizing a compiled dataset of 400 boreholes, spatial distributions were modeled. The contour map from the aquifer to DCS site is plotted using Kriging interpolation (Figure 5).
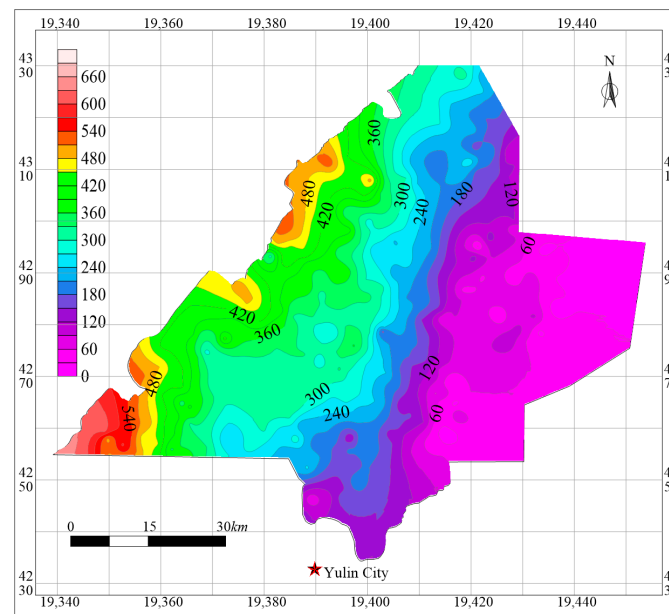
Figure 5. Distance from DCS site to Salawusu Formation aquifer.

(3)   Equivalent permeability of protective zone

The engineering parameters of 30–10 m, where the width of GCSS (WGCSS) and CMSS (WCMSS) are 30 and 10 m, respectively, were taken for example. The HWCFZ of DCS is as follows [34]:

$$H_f = 5.60h + 0.013d + 17.86 \sum_{i=0}^{i=m} T_i/d + 29.02 \ln w_g - 2.68 w_m - 61.6 \quad R^2 = 0.92 \qquad (20)$$

where T_i is the thickness of the *i-th* overlying stratum; w_g and w_m are the WGCSS and WCMSS, respectively.

Based on the on-site measurement results of drilling and pumping tests in the Yu-Shen mining area, the initial permeability coefficients of overlying strata are listed in Table 3. The post-engineering permeability coefficients of different stratigraphic combination structures are further merged and determined by referring to the COMSOL multi-field coupling simulation (COMSOL Multiphysics 6.0, COMSOL Software Technology (Shanghai) Co., Ltd., Shanghai, China) (Table 4).

Table 3. Initial permeability coefficient of overlying rocks.

Strata	Initial Permeability Coefficient (cm/s)
Clay	2.0×10^{-8}
Loess	3.0×10^{-5}
Siltstone	8.0×10^{-4}
Fine sandstone	3.5×10^{-3}
Medium sandstone	1.3×10^{-2}
Coarse sandstone	4.0×10^{-2}

Table 4. Post-engineering permeability coefficient of overlying rocks.

Strata	Initial Permeability Coefficient (cm/s)
Sand	1.3×10^{-4}
Soil	1.2×10^{-7}
Bedrock	5.8×10^{-3}

The equivalent permeability coefficient of the protective zone under different schemes is calculated by using Equation (7). The Kriging method is then employed to draw the contour map of the equivalent permeability coefficient after DCS operation, as shown in Figure 6.

(**a**)

(**b**)
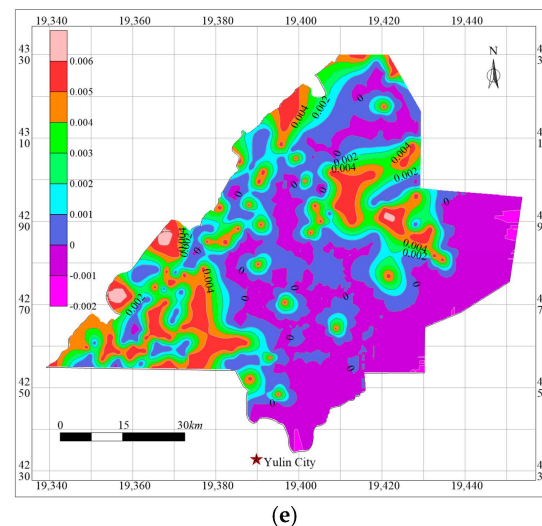
(**c**)

(**d**)

Figure 6. *Cont.*

(**e**)
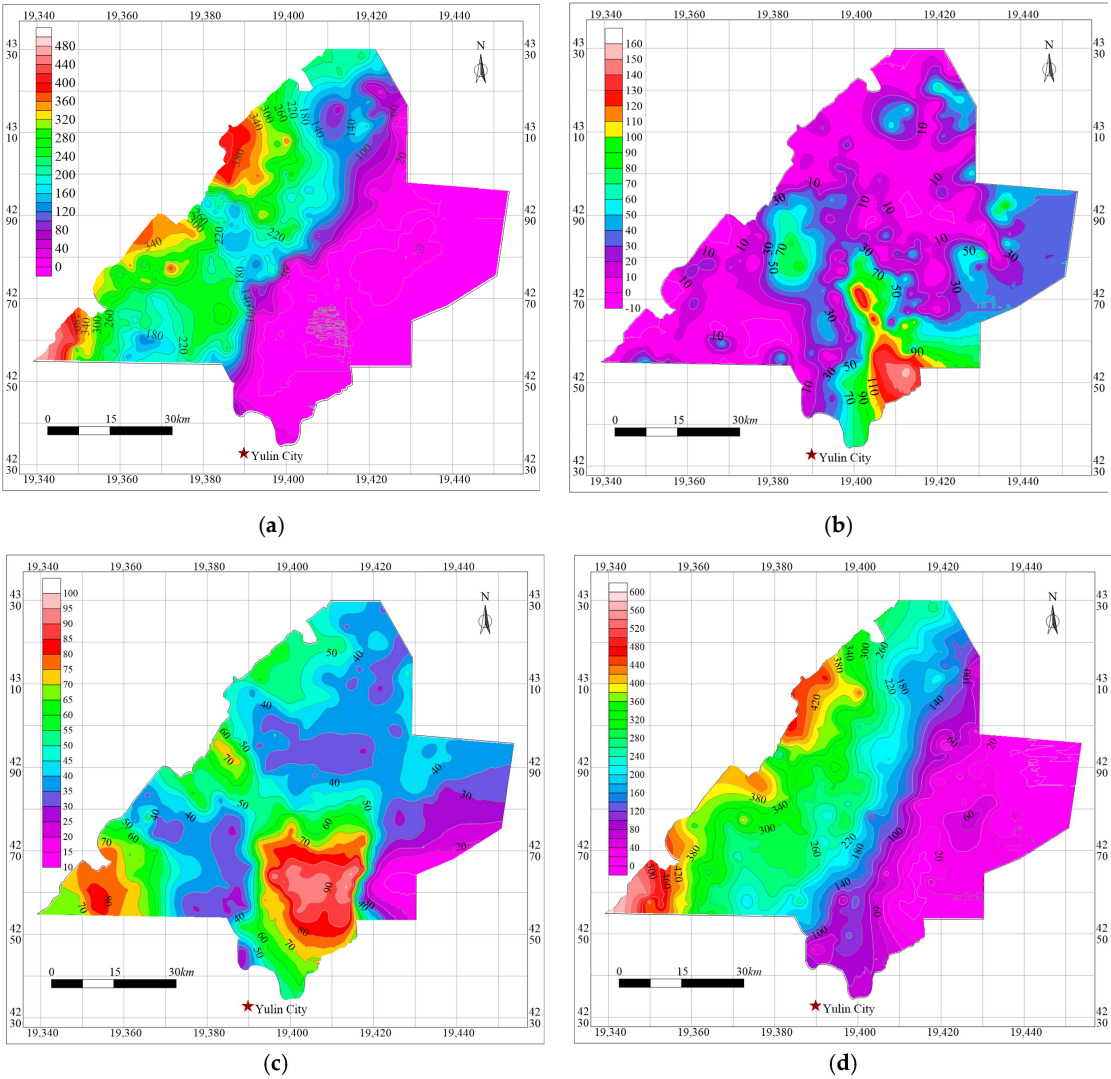
Figure 6. Contour maps of equivalent permeability system. (**a**) thickness of bedrock; (**b**) thickness of aquifuge (clay); (**c**) HWCFZ (30–10 m); (**d**) thickness of undamaged strata (30–10 m); (**e**) equivalent permeability coefficient of undamaged strata (30–10 m).

5.1.3. UCS of CMBM

The CMBM were prepared using CG as an aggregate while low-calcium FA, cement, CO_2 gas, silicate additive, etc., were the raw materials [42]. The cement proportion was set as 20 wt% while the FA content was set as 20%, 40%, 60%, and 80%, respectively. The concentration of Na_2SiO_3 solution was determined at 15 wt% as 10 wt% is insufficient to support CG particles. Moreover, good fluidity is necessary to ensure that CO_2 can react with the fresh slurry completely through bubbling. Therefore, the solid–liquid ratio was determined to be 2:0.8.

Compressive strength and UCS development of CMBM are presented in Figure 7. Comprehensive analysis of UCS in CMBM reveals that both fly ash content and curing time exert significant positive effects on mechanical performance. UCS consistently increased with prolonged curing across all FA levels, attributable to progressive carbonation reactions forming densifying carbonate precipitates [43]. Crucially, a pronounced synergistic interaction was observed: higher FA content substantially amplified the strength gain over time. Specifically, the 3 d to 56 d UCS increase escalated from 179% (20% FA) to 350% (80% FA). Similarly, the strength enhancement from 20% to 80% FA intensified from 31% at 3 d to 111% at 56 d. This synergy stems from the dual role of fly ash as a long-term reactant reservoir (providing Ca^{2+} and Mg^{2+} for carbonate formation) and a micro-filler, with optimal performance (UCS up to 7.52 MPa) achieved at 80% FA after 56-day curing. These findings demonstrate that extended curing maximizes the efficacy of high-volume FA in CO_2 mineralization systems, significantly enhancing late-age strength development through sustained pozzolanic and carbonation reactions [44].

5.2. Prediction Results of DCS Suitability

Based on the composite evaluation index Φ computed for 400 boreholes, a contour map illustrating the suitability of DCS within the Yu-Shen mining area was generated via Kriging interpolation, as depicted in Figure 8.

Overall, the adaptability ratings in the northwestern sectors are generally superior to those in the east. Two distinct Grade I zones were identified, each spatially discontinuous and located in the northwestern, southwestern, and central portions of the coal field. These areas are characterized by favorable DCS conditions, stable floor conditions, thick aquifuge, and simple geological structures. Such conditions allow for the direct application of DCS

without additional measures, thereby simultaneously ensuring the safety of CO_2 storage, infrastructure protection, and environmental preservation. Areas classified as Grade II are primarily situated along the northeastern parts of the mining zone. Mines within these regions can implement the DCS by incorporating minor supplemental engineering strategies, enabling a synergistic approach that balances carbon sequestration, aquifer integrity, and the management of coal-related solid waste.
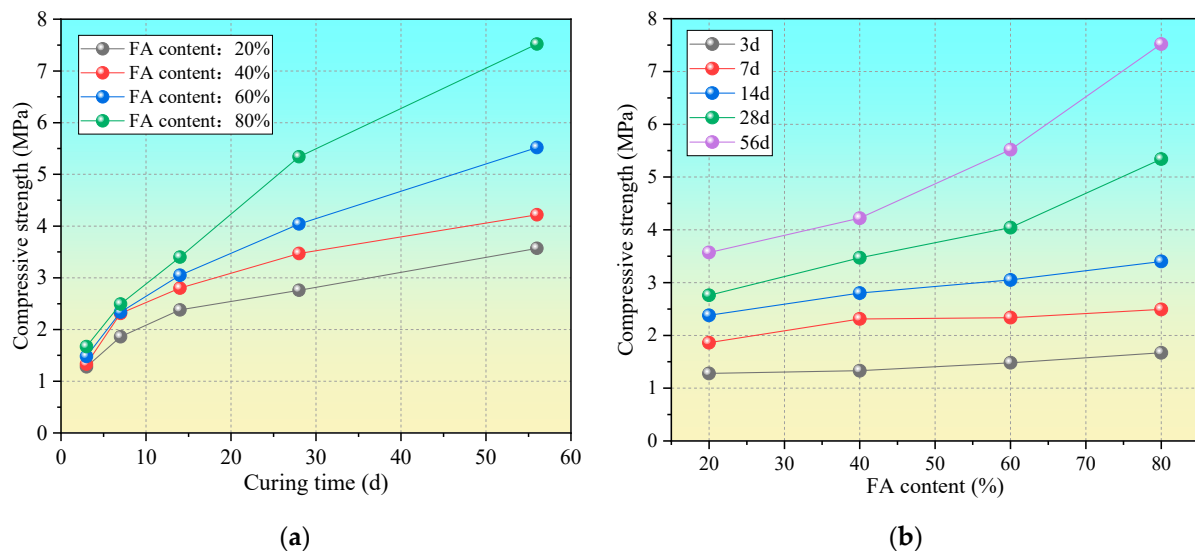

Figure 7. Influence of curing time and FA content on CMBM strength. (**a**) Curing time; (**b**) FA content.
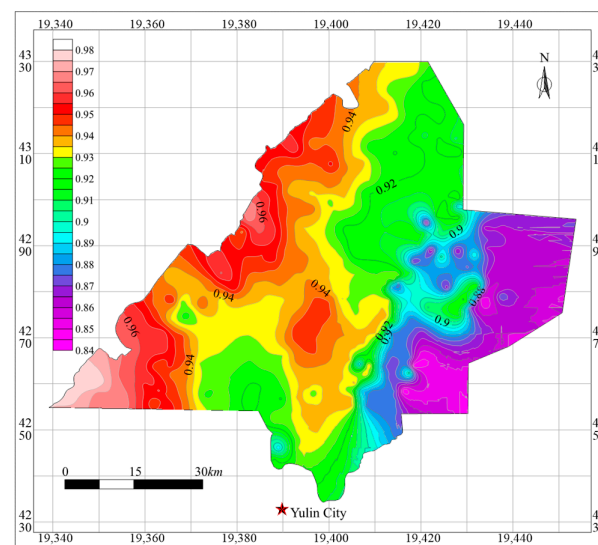
Figure 8. Contour map of DCS appropriateness in Yu-Shen coal area.

6. Discussion

(1) This research pushes the frontiers of carbon sequestration technology while simultaneously transforming the perceived function of coal mines within a low-carbon economy. It illustrates a synergy between advanced engineering and environmental responsibility, showcasing how legacy industrial infrastructure can be repurposed for sustainable ends. Beyond advancing CO_2 sequestration techniques, this work recasts coal mines as assets for a low-carbon future, merging innovative engineering with ecological care to convert industrial relics into tools for sustainability. A significant barrier to the widespread adoption of DCS is the absence of universally accepted benchmarks for evaluating storage efficiency, coupled with the lack of a

comprehensive, cross-disciplinary regulatory framework. These interconnected gaps currently impede the scalability of the technology and hinder its large-scale deployment. The insights and conclusions presented in this study directly address these challenges. They provide not only a practical framework and actionable strategies for implementing DCS on a broader scale but also establish a foundational theoretical basis. This contribution is designed to inform and guide the subsequent development of robust governance structures, necessary legislation, and effective policy-making for this promising technology.

(2) Utilizing abandoned mine voids for supercritical CO_2 sequestration leverages existing subsurface volume but introduces complex geomechanical and hydrogeological challenges. Bulk gas emplacement provides immediate volumetric uptake but remains vulnerable to buoyancy-driven migration and leakage through imperfect seals or legacy discontinuities, thereby requiring sustained pressure management and long-term monitoring to establish containment integrity. In situ carbonation confers higher chemical permanence by converting CO_2 to stable carbonate phases, yet its field-scale efficacy is limited by slow reaction kinetics, constrained reactive mineral availability, and mass-transfer bottlenecks, which together suppress the fraction of CO_2 mineralized within operationally relevant timescales. The amount of CO_2 stored by pure mineralization is only 0.07% of what the DCS approach can achieve. The DCS approach seeks to reconcile these tendencies by coupling short-term mechanical containment of a gaseous subspace with progressive mineralization in an adjacent mineralized subspace. Performance is highly site-dependent and controlled by host-rock mineralogy, native gas inventories and pore pressures, structural complexity, and engineered parameters such as void utilization, injection sequencing, and pressure control. Mechanistically, net retention reflects the evolving balance between WGCSS and WCMSS; under tightly managed, favorable conditions (high void use, accelerated carbonation pathways, and stringent pressure regulation), DCS efficiency can reach roughly 76% of that attainable by single-mode gas emplacement. Importantly, the hybrid approach does not eliminate leakage or kinetic constraints; robust implementation therefore requires targeted site selection, coupled flow–transport–reaction–geomechanical modeling calibrated by pilot data, engineered backfilling and compartmentalized injection strategies, and a multiparameter, long-term verification program capable of resolving the temporal evolution of GCSS, CMSS, mineralization rates, and potential leakage pathways.

(3) The principal strength of the developed assessment framework lies in the adaptability of its methodological structure. When applied to diverse geological settings, such as high-gas or structurally complex mining areas, the model can be contextually calibrated through the modification of evaluation indicators and their corresponding weighting factors. However, it is imperative to acknowledge its constraints: under such challenging geotechnical conditions, inherent geological uncertainties are amplified, substantially elevating the prerequisites for long-term sealing integrity and operational safety. These factors may critically compromise both the technical viability and economic feasibility of project implementation. Consequently, the model serves primarily as a high-tier screening tool for regional-scale preliminary evaluation, effectively prioritizing areas warranting subsequent, site-specific investigations and detailed risk assessments.

(4) Although the evaluation framework developed in this study integrates multiple factors, it does not yet account for the effects of cyclic mechanical loading and groundwater interaction on CO_2 mineralized backfill materials. In future work we will undertake a systematic investigation of how cyclic loading and groundwater expo-

sure influence the materials' microstructure and phase/morphological characteristics, and how these processes contribute to mechanical degradation, particularly water-induced weakening.

7. Conclusions

The main conclusions are as follows:

(1)　A groundbreaking DCS methodology was conceptualized to repurpose abandoned coal mines into active carbon repositories. This technique synergizes CO_2 storage with carbonation processes using backfill materials, creating a multifaceted solution to pressing environmental issues. It presents a unified strategy for achieving carbon neutrality, managing industrial solid waste, and conserving vital water resources. The research establishes a scalable framework for transforming post-mining landscapes into carbon-negative systems, thereby counteracting long-term ecological damage.

(2)　The CMBM was fabricated through a reaction between CO_2 and coal-based solid wastes (FA and CG), conducted under standard atmospheric temperature and pressure conditions. An indoor testing regime was conducted to evaluate the uniaxial compressive strength (UCS) of the CMBM samples. The results show that both FA content and curing time significantly enhance mechanical performance. Across all FA levels, UCS increased consistently with prolonged curing due to progressive carbonation reactions that form densifying carbonate precipitates. A pronounced synergistic interaction was observed, wherein a higher FA content substantially amplified the strength gain over time; the UCS increase from 3 to 56 days escalated from 179% at 20% FA to 350% at 80% FA. Similarly, the strength improvement from increasing FA from 20% to 80% intensified from 31% at 3 days to 111% at 56 days. This synergy originates from the dual role of fly ash, which serves as a long-term reservoir of reactive ions (Ca^{2+} and Mg^{2+}) for carbonate formation and provides a micro-filling effect. The optimal performance, with a UCS of up to 7.52 MPa, was achieved with 80% FA after a 56-day cure. These findings confirm that extended curing durations maximize the efficacy of high-volume FA in CO_2 mineralization systems, facilitating considerably greater late-age strength development through sustained pozzolanic and carbonation reactions.

(3)　An AHP integrated with a fuzzy comprehensive evaluation was deployed to establish a three-tiered predictive model to assess the suitability of DCS. The framework incorporates four secondary indicators and twelve tertiary indicators as influential factors. A detailed analysis was performed to determine the weight distribution and corresponding membership functions for each factor. The results from this weighting analysis reveal that among the secondary indicators, the geological structure system is the most significant determinant, with a calculated weight of 0.6095. The DCS site system and hydrogeological system are jointly identified as the next most critical factors, each assigned a weight of 0.2092 and 0.1095, respectively. At the more detailed tertiary level, the fault strength emerges as the paramount indicator, carrying a weight of 0.3335.

(4)　The developed predictive model was generalized and applied to conduct a suitability assessment across the Yu-Shen mining area. Thematic maps were generated for each individual evaluation factor to visually represent spatial variations and to calculate the membership degree for every indicator at various locations. This geospatial analysis facilitated the calculation of a comprehensive adaptability index for 400 specific boreholes distributed throughout the coal field. Subsequently, the Kriging geostatistical interpolation technique was employed to create a zoning map, delineating areas of high and medium suitability across the entire mining region. The resulting predic-

tion and spatial visualization provide a critical theoretical foundation and a practical decision-support tool for future field-scale implementation of DCS technology.

Abbreviations

The following abbreviations are used in this manuscript:

DCS	Dual CO_2 storage
CMBM	CO_2 mineralized backfill material
CMSS	CO_2 mineralized storage segment
GCSS	Gaseous CO_2 storage segment
AHP	Analytic hierarchy process
FA	Fly ash
CG	Coal gangue
WGCSS	Width of gaseous CO_2 storage segment
WCMSS	Width of CO_2 mineralized storage segment
HWCFZ	Height of water-conducting fractured zone

References

1. Wu, L.; Qi, G.; Lu, W.; He, Z.; He, M. Study on Preparation and performance of calcium carbide slag foam for coal mine disaster reduction and CO_2 storage. *Colloid Surface A* **2020**, *606*, 125322. [CrossRef]

2. Li, Q.S. The view of technological innovation in coal industry under the vision of carbon neutralization. *Int. J. Coal Sci. Technol.* **2021**, *8*, 1197–1207. [CrossRef]

3. Li, W.; Ren, T.W.; Su, E.L.; Cheng, Y. Is the long-term sequestration of CO_2 in and around deep, abandoned coal mines feasible? *Proc. Inst. Mech. Eng. Part A J. Power Energy* **2018**, *232*, 27–38. [CrossRef]

4. Du, Q.H.; Liu, X.L.; Wang, E.Z.; Wang, S.J. Strength Reduction of Coal Pillar after CO_2 Sequestration in Abandoned Coal Mines. *Minerals* **2017**, *7*, 26. [CrossRef]

5. Wang, X.L.; Gao, S.W.; Liu, L.B.; Cai, M.; Wang, J. A novel process of capture and utilize carbon dioxide from coal-fired power plant to product high value product. *Proc. CSEE* **2012**, *32*, 164–167. [CrossRef]

6. Li, Q.C.; Li, Q.; Wu, J.J.; He, K.G.; Xia, Y.F.; Liu, J.Y.; Wang, F.L.; Cheng, Y.F. Wellhead Stability During Development Process of Hydrate Reservoir in the Northern South China Sea: Sensitivity Analysis. *Processes* **2025**, *13*, 1630. [CrossRef]

7. Li, Q. Reservoir Science: A Multi-Coupling Communication Platform to Promote Energy Transformation, Climate Change and Environmental Protection. *Reserv. Sci.* **2025**, *1*, 1–2. [CrossRef]

8. Gao, X.D.; Zhang, K.; Ji, D.Q.; Ma, H.M.; Meng, Y.; Jiang, S.; Tian, W.; Tang, Y.H.; He, L.; Liu, C.H.; et al. A proposed layout of CO_2 capture utilization and storage for coal fired power plants in China. *Fuel* **2025**, *401*, 15. [CrossRef]

9. Bobicki, E.R.; Liu, Q.; Xu, Z.; Zeng, H. Carbon capture and storage using alkaline industrial wastes. *Prog. Energ. Combust.* **2012**, *38*, 302–320. [CrossRef]

10. Thanh, H.V.; Yasin, Q.; Al-Mudhafar, W.J.; Lee, K.-K. Knowledge-based machine learning techniques for accurate prediction of CO_2 storage performance in underground saline aquifers. *Appl. Energy* **2022**, *314*, 118985. [CrossRef]

11. Kim, Y.; Jang, H.; Kim, J.; Lee, J. Prediction of storage efficiency on CO_2 sequestration in deep saline aquifers using artificial neural network. *Appl. Energy* **2017**, *185*, 916–928. [CrossRef]

12. Ahmadi, M.A.; Kashiwao, T.; Rozyn, J.; Bahadori, A. Accurate prediction of properties of carbon dioxide for carbon capture and sequestration operations. *Pet. Sci. Technol.* **2016**, *34*, 97–103. [CrossRef]

13. Thanh, H.V.; Sugai, Y.; Nguele, R.; Sasaki, K. Integrated workflow in 3D geological model construction for evaluation of CO_2 storage capacity of a fractured basement reservoir in Cuu Long Basin, Vietnam. *Int. J. Greenh. Gas Control* **2019**, *90*, 102826. [CrossRef]

14. He, L.P.; Shen, P.P.; Liao, X.W.; Gao, Q.C.; Wang, C.S.; Li, F.F. Study on CO_2 EOR and its geological sequestration potential in oil field around Yu lin city. *J. Pet. Sci. Eng.* **2015**, *134*, 199–204. [CrossRef]

15. Pratama, E.; Ismail, M.S.; Ridha, S. Identification of coal seams suitability for carbon dioxide sequestration with enhanced coalbed methane recovery: A case study in South Sumatera Basin, Indonesia. *Clean Technol. Environ. Policy* **2017**, *20*, 581–587. [CrossRef]

16. Thanh, H.V.; Sugai, Y.; Sasaki, K. Application of artificial neural network for predicting the performance of CO_2 enhanced oil recovery and storage in residual oil zones. *Sci. Rep.* **2020**, *10*, 18204. [CrossRef]

17. Deveci, M.; Demirel, N.Ç.; John, R.; Özcan, E. Fuzzy multi-criteria decision making for carbon dioxide geological storage in Turkey. *J. Nat. Gas Sci. Eng.* **2015**, *27*, 692–705. [CrossRef]

18. Olajire, A.A. A review of mineral carbonation technology in sequestration of CO_2. *J. Pet. Sci. Eng.* **2013**, *109*, 364–392. [CrossRef]

19. Woodall, C.M.; McQueen, N.; Pilorgé, H.; Wilcox, J. Utilization of mineral carbonation products: Current state and potential. *Greenh. Gases* **2019**, *9*, 1096–1113. [CrossRef]

20. Brent, G.F.; Allen, D.J.; Eichler, B.R.; Petrie, J.G.; Mann, J.P.; Haynes, B.S. Mineral Carbonation as the Core of an Industrial Symbiosis for Energy-Intensive Minerals Conversion. *J. Ind. Ecol.* **2012**, *16*, 94–104. [CrossRef]

21. Liu, W.Z.; Teng, L.M.; Rohani, S.; Qin, Z.F.; Zhao, B.; Xu, C.C.; Ren, S.; Liu, Q.C.; Liang, B. CO_2 mineral carbonation using industrial solid wastes: A review of recent developments. *Chem. Eng. J.* **2021**, *416*, 129093. [CrossRef]

22. Xu, Y.J.; Ma, L.Q.; Wang, Y.Y.; Zhai, J.T.; Zhao, Z.Y. Strata migration and fracture development under continuous extraction and continuous backfill with CO_2 mineralized backfill materials. *Geomech. Geophys. Geo.* **2025**, *11*, 50. [CrossRef]

23. Cwik, A.; Casanova, I.; Rausis, K.; Koukouzas, N.; Zarebska, K. Carbonation of high-calcium fly ashes and its potential for carbon dioxide removal in coal fired power plants. *J. Clean Prod.* **2018**, *202*, 1026–1034. [CrossRef]

24. Mo, L.W.; Zhang, F.; Deng, M.; Panesar, D.K. Effectiveness of using CO_2 pressure to enhance the carbonation of Portland cement-fly ash-MgO mortars. *Cement Concrete Com.* **2016**, *70*, 78–85. [CrossRef]

25. Liu, W.; Su, S.; Xu, K.; Chen, Q.D.; Xu, J.; Sun, Z.J.; Wang, Y.; Hu, S.; Wang, X.L.; Xue, Y.T.; et al. CO_2 sequestration by direct gas-solid carbonation of fly ash with steam addition. *J. Clean Prod.* **2018**, *178*, 98–107. [CrossRef]

26. Ukwattage, N.L.; Ranjith, P.G.; Yellishetty, M.; Bui, H.H.; Xu, T. A laboratory-scale study of the aqueous mineral carbonation of coal fly ash for CO_2 sequestration. *J. Clean Prod.* **2015**, *103*, 665–674. [CrossRef]

27. Ashraf, W. Carbonation of cement-based materials: Challenges and opportunities. *Constr. Build. Mater.* **2016**, *120*, 558–570. [CrossRef]

28. Luo, S.Q.; Gao, S.; Yang, L.; Liu, S.H.; Guan, X.M.; Wang, D.Q. Enhancing coal gangue aggregates with fly ash-cement slurry: Synergistic effects of CO_2 mineralization on physical and mechanical properties. *Constr. Build. Mater.* **2024**, *440*, 137389. [CrossRef]

29. Wu, H.F.; Liu, Y.; Li, H.; Wang, K.; Guo, Y.L. Effects of carbonization on gangue-cemented paste backfill properties. *Int. J. Green Energy* **2021**, *18*, 282–296. [CrossRef]

30. Liu, L.; Xia, L.; Fang, Z.Y.; Jia, Q.F.; Gao, Y.H.; He, W.; Liu, Z.Z. Performance study of modified magnesium-coal based solid waste negative carbon backfill material: Strength characteristics and carbon fixation efficiency. *J. Environ. Chem. Eng.* **2024**, *12*, 113281. [CrossRef]

31. Ngo, I.; Ma, L.Q.; Zhai, J.T.; Wang, Y.Y. Enhancing fly ash utilization in backfill materials treated with CO_2 carbonation under ambient conditions. *Int. J. Min. Sci. Technol.* **2023**, *33*, 323–337. [CrossRef]

32. Xu, Y.J.; Ma, L.Q. Characteristics of overburden migration under continuous extraction and continuous backfill mining method with CO_2 mineralized filling materials. *J. Clean Prod.* **2024**, *440*, 140920. [CrossRef]

33. Xu, Y.J.; Ma, L.Q.; Wang, L.; Ngo, I.; Wang, Y.Y. Continuous extraction and continuous backfill for gaseous and mineralized dual CO_2 sequestration and water-preserving coal mining. *Geomech. Geophys. Geo.* **2025**, *11*, 40. [CrossRef]

34. Xu, Y.J. Protective Mechanism and Control of Overlying Water-Seepage-Resistance Strata Under Continuous Extraction and Continuous Backfill. Ph.D. Dissertation, China University of Mining and Technology, Xuzhou, China, 2023. [CrossRef]

35. Lian, X.; Hu, H.; Li, T.; Hu, D. Main geological and mining factors affecting ground cracks induced by underground coal mining in Shanxi Province, China. *Int. J. Coal Sci. Technol.* **2020**, *7*, 362–370. [CrossRef]

36. Liu, J.W.; Sui, W.H.; Zhao, Q.J. Environmentally sustainable mining: A case study of intermittent cut-and-fill mining under sand aquifers. *Environ. Earth Sci.* **2017**, *76*, 562. [CrossRef]

37. Liu, Y.; Eckert, C.M.; Earl, C. A review of fuzzy AHP methods for decision-making with subjective judgements. *Expert Syst. Appl.* **2020**, *161*, 113738. [CrossRef]

38. Saaty, T.L.; Beltran; Miguel, H. Architectural Design by the Analytic Hierarchy Process. *Des. Methods Theor.* **1980**, *14*, 124–134.

39. Saaty, T.L. *The Application of Analytic Hierarchy Process in Resource Allocation, Management and Conflict Analysis*; Coal Industry Press: Beijing, China, 1988; Volume 334.

40. Gupta, S.; Kumar, U. An analytical hierarchy process (AHP)-guided decision model for underground mining method selection. *Int. J. Min. Reclam. Environ.* **2012**, *26*, 324–336. [CrossRef]

41. Gao, T.; Wang, X.Q.; Wang, H.Y.; Gu, C.; Zhou, Z.Y.; Yang, Z. A Study on the Breakthrough Pressure of Porous Rock Formations in Gas Storage Reservoirs. *Processes* **2024**, *12*, 2193. [CrossRef]

42. Guo, Y.M.; Zhang, J.X.; Long, K.; Ma, J.Y.; Gao, Y.; Li, B.Y. Experimental study on CO_2 sequestration capacity and mechanical characteristics evolution of solid wastes based carbon-negative backfill materials. *Constr. Build. Mater* **2024**, *440*, 137457. [CrossRef]

43. Zhao, Y.; Taheri, A.; Karakus, M.; Chen, Z.W.; Deng, A. Effects of water content, water type and temperature on the rheological behaviour of slag-cement and fly ash-cement paste backfill. *Int. J. Min. Sci. Technol.* **2020**, *30*, 271–278. [CrossRef]

44. Shaladi, R.J.; Johari, M.A.M.; Ahmad, Z.A.; Mijarsh, M.J.A. The engineering properties and pozzolanic reaction kinetics of quaternary blended binder high strength mortars optimized by the Taguchi method. *J. Build. Eng.* **2022**, *54*, 104582. [CrossRef]